Exciton-exciton annihilation and exciton kinetics in poly(di-*n*-hexylsilane)

R. G. Kepler
Sandia National Laboratories, Albuquerque, New Mexico 87185

Z. G. Soos
Department of Chemistry, Princeton University, Princeton, New Jersey 08544

(Received 13 July 1992)

We have found that charge carriers can be generated by exciton-exciton annihilation in solid films of poly(di-*n*-hexylsilane). We use this phenomenon to study the kinetics of excitons at ambient temperature and show that the rate constant for exciton-exciton annihilation γ is 2×10^{-7} cm^3 s^{-1}, in excellent agreement with the value we obtained previously by other means. The quantum efficiency for carrier production, at an electric field of 2×10^5 V cm^{-1}, is 1.3×10^{-3} per annihilation event. We also show that γ is independent of the initial energy of the exciton state, even to energies far out on the long-wavelength tail of the exciton absorption band, and that the excitons remain mobile throughout their 600-ps lifetime.

I. INTRODUCTION

The recent observation of electroluminescence in polymers and the possibility that light-emitting diodes might be made from solution-cast polymer films[1,2] have lead to increased interest in the nature of excitons in polymers. We have been studying the electronic states of polysilanes[3,4] and recently discovered that charge carriers can be generated by exciton-exciton annihilation in poly(di-*n*-hexylsilane) (PDHS).[5] This observation provides a tool for the study of exciton kinetics in polymers.

Polysilanes are σ-conjugated polymers which exhibit many properties quite similar to those of the more familiar π-conjugated polymers. In polysilanes the first absorption band is at a much lower energy than initially expected for a σ-bonded material,[6] the fluorescence quantum efficiency is quite high,[7] and they are excellent photoconductors.[8,9] These properties are a consequence of σ-electron delocalization along the silicon backbone. The electronic states can be well described by including Coulomb interactions and using the Sandorfy C model,[10] a modification of the Hückel model, for σ conjugation in which the transfer integrals $t(1\pm\delta)$ alternate because one integral is between sp^3 orbitals on different silicon atoms and the other is between sp^3 orbitals on the same silicon atom.[3,11] The theory[11] is essentially the same as the one describing π-conjugated polyenes, but with parameters for silicon rather than carbon.

The absorption spectra, typically broad, featureless bands showing no evidence for vibrational fine structure, are usually interpreted in terms of excited states of segments of the polymer chains, and it is assumed that the spectra are inhomogeneously broadened by distributions of segment lengths.[6] Quantitative agreement with temperature-dependent absorption spectra[7,12] and a rod-to-coil transition which occurs in some polysilanes have been obtained with models of this type.[12]

The fluorescence band is narrower than the absorption band and just below it in energy.[7] When polarized light is used to excite fluorescence in dilute solution or glasses, the fluorescence is partially polarized if the excitation is in the first absorption band and the amount of polarization increases toward the low-energy portion of the band.[13,14] Time-dependent measurements of fluorescence depolarization in solution and glasses[15,16] have shown an initial rapid decay, 20–30 ps, followed by a slow decay of about 2 ns. The amount of residual polarization remaining after the initial decay depends on the excitation wavelength and is near the theoretical maximum when the excitation is on the low-energy side of the absorption band. These observations have led to the conclusion that energy moves quickly from the initially excited segment to longer, lower-energy segments where it becomes trapped until a photon is emitted.

Site-selective fluorescence studies[17] and hole-burning experiments[18] have been conducted on solid films of polysilanes at low temperatures. The site-selective fluorescence studies involved measurements of the fluorescence excited by photons with energies in the red edge of the exciton absorption band, and it was concluded that at very low temperatures and far out on the red edge, where only longer segments were excited, the excited state was localized on the excited segment and the Stokes shift was less than 20 cm^{-1}, the experimental resolution. In the hole-burning experiments, it was found that the photolyzed segments are parallel, within experimental error, to the absorbing ones, and it was concluded that energy transfer occurs between segments within a crystallite but not between crystallites.

In earlier work,[19–21] we studied exciton kinetics by measuring the intensity of fluorescence versus exciting light intensity and interpreted nonlinearities observed at high intensities as due to exciton-exciton annihilation. In that work it was concluded that the exciton-exciton annihilation rate constant γ is about 1×10^{-7} cm^3 s^{-1} in PDHS, that it is about the same in poly(methylphenylsilane) and poly(*n*-propylmethylsilane), and that it is independent of temperature in poly(*n*-propylmethylsilane) down to 20 K. These results indicate that excitons are highly mobile in polysilane films and

that they remain mobile down to low temperatures.

The work reported in this paper, which addresses some of the above hypothesis, was originally undertaken to determine the quantum efficiency for carrier generation as a function of photon energy and thus determines the magnitude of the free-carrier band gap in poly(di-*n*-hexylsilane) (PDHS). We have been unable to find clear evidence for a distinct free-carrier band edge. Single-photon processes become observable near 4.5 eV but the quantum efficiency for carrier generation continues to rise rapidly well above 5 eV. The highest energy data suggests that the band gap is 5.2 eV.

The scope of this work broadened considerably when we discovered that charge carriers were being created by a nonlinear process at photons energies less than 4.5 eV. As we report here and in earlier discussions of preliminary results,[5,22,23] investigations of this process have shown that carriers can be generated by exciton-exciton annihilation and that the exciton-exciton annihilation rate constant is in excellent agreement with that determined previously from measurements of fluorescence intensity versus exciton density. The annihilation rate constant is independent of the energy used to create the excitons within experimental error, even to energies on the low-energy side of the exciton band where the absorption coefficient is near 100 cm^{-1}, down from about 10^5 cm^{-1} at the peak of the absorption band. All the measurements reported here were made in ambient temperature.

The rest of the paper is organized as follows. The next section, Sec. II, describes the experimental techniques used and is followed by a section on the kinetic equation used to interpret the results. In Sec. IV, the experimental results are presented. Section V is a discussion of the significance of the results and the final section is a short summary.

II. EXPERIMENT

Standard time-of-flight photoconductivity techniques were used to determine the photon energy dependence of the carrier generation quantum efficiency. In this technique a thin, high-resistivity, photoconducting film is placed in a high electric field between two electrodes. A pulse of light generates carriers in the film which drift to the electrodes in the applied field. Previous experiments on polysilanes have shown that only holes are mobile and that they readily drift the distance required to reach the electrodes with little trapping.[8,9] The charge displaced on the electrodes in this experiment is equal to the electronic charge times the distance of carrier travels, divided by the thickness of the film.

Semitransparent aluminum electrodes were vacuum deposited on UV fused quartz substrates and polymer films were cast from toluene solution onto the electrode. A second, thick aluminum electrode was vacuum deposited on the polymer film. Polymer film thicknesses from a few micrometers to about 20 μm were used. Most of the data reported were obtained using a single 3.4-μm-thick sample. Electric fields equal to 2×10^5 V cm^{-1} were applied and the amount of charge displaced on the electrodes by a pulse of light was measured with a charge sensitive preamplifier, with an electrometer or with an oscilloscope using a circuit with an RC time constant which was long compared to the length of the light pulse and to the transit time of the carriers.

Most measurements were made with two different laser light sources. One was a dye laser which provided light pulses about 5 ns long of variable wavelength. The other was a tripled Nd:YAG (where YAG denotes yttrium aluminum garnet) which provided nominally 30-ps light pulses at 355 nm. The light intensity in both experiments was controlled with two polarizers by rotating the plane of polarization of the polarizer closest to the light source. To exclude exciton-exciton annihilation, some experiments were conducted at very low light intensities by using light from xenon and deuterium arcs which had passed through a monochromator. A sample approximately 20 μm thick was used. A shutter turned the light on for 20 s and the steady-state current was measured with an electrometer.

The dye laser was used to determine the photon energy and light intensity dependence of the number of carriers generated. The 30-ps pulses at 355 nm were used to measure the number of carriers generated in a series of double-pulse experiments in which the sample was irradiated by two equal intensity light pulses separated in time by a variable delay. As will be explained later, this experiment required operating at as low a light intensity as possible. Charge sensitive preamplifiers were used to integrate the charge displaced and the preamplifiers allowed us to make measurements below 10^6 electrons displaced.

III. KINETIC EQUATION

All the data on carrier generation will be analyzed using the rate equation

$$\frac{dn}{dt}=G(z,t)-\beta n-\gamma n^2 . \tag{1}$$

Here $n(r)$ is the exciton concentration, G is the rate of exciton generation, β is the reciprocal of the exciton lifetime, and γ is the exciton-exciton annihilation rate constant. We assume that exciton-exciton annihilation produces a highly excited state that decays into charge carriers with some quantum efficiency η. In previous studies on PDHS and other silanes, we used Eq. (1) to describe the fluorescence intensity as a function of $n(r)$ for both one- and two-photon excitation.[19–21] These studies showed that $\gamma\sim1\times10^{-7}$ cm^3 s^{-1}. The exciton lifetime in PDHS, determined from measurements of fluorescence intensity versus time on our material, is $1/\beta=600$ ps. The quantum efficiency for carrier generation following exciton-exciton annihilation, η, is consequently the only new parameter.

The steady-state and pulsed photoconductivity experiments thus provide stringent tests for the applicability of Eq. (1). There are only two decay channels, independent of energy. We will further simplify to a one-dimensional problem in the film thickness, $0<z<d$, and take a laser spot $A=0.4$ cm^2 with uniform intensity. The intensity profile of the laser is not critical for one-photon absorp-

tion, as found for the photoconduction, and variations of linear contributions largely cancel.

In the double-pulse experiments, the sample was irradiated with two 30-ps-long pulses superimposed in space, but separated by a variable time delay Δt. Since the pulses are short compared to the 600-ps exciton lifetime, we model them as delta functions. The initial density $n(z,0)$ of excitons at depth z generated by a pulse is

$$n(z,0)=\alpha I_0 \tau e^{-\alpha z} \quad (0<z<d) , \tag{2}$$

where d is the film thickness, τ the pulse length, and I_0 is the intensity of the incident light in photons $\mathrm{cm}^{-2}\mathrm{s}^{-1}$. The time evolution under Eq. (1) gives

$$n(z,t)=\frac{n(z,0)e^{-\beta t}}{1+B(z,0)(1-e^{-\beta t})} \tag{3}$$

with $B(z,0)=n(z,0)\gamma/\beta$. The total number of carriers generated at depth z is the time integral of $\eta\gamma n(z,t)^2$,

$$q(z)=\left[\frac{\eta A\beta}{\gamma}\right]\{B(z,0)-\ln[1+B(z,0)]\} . \tag{4}$$

The total number of carriers generated by a single pulse is the integral of $q(z)$ over the film thickness.

A second pulse of the same intensity is applied at $t=\Delta t$. The exciton density due to both pulses is

$$N(z,\Delta t)=n(z,\Delta t)+n(z,0) . \tag{5}$$

The total number of carriers generated for $t>\Delta t$ is then given by Eq. (4) with $B(z,0)=N(z,\Delta t)\gamma/\beta$. We must still add the carriers $q(z,\Delta t)$ generated by the first pulse prior to Δt. After some algebra, the total number of carriers $Q(z,\Delta t)$ generated at depth z is found to be

$$Q(z,\Delta t)=2q(z)-\frac{\eta A\beta}{\gamma}\ln[1-H(z,\Delta t)] \tag{6}$$

with

$$H(z,\Delta t)=\frac{e^{-\beta\Delta t}B(z,0)^2}{[1+B(z,0)]^2} . \tag{7}$$

As expected, H vanishes for $\Delta t \gg 1/\beta$. It also follows, for $\Delta t=0$ and $B(z,0)\ll 1$, that coincident weak pulses lead to $Q(z,0)=4q(z,0)$.

The integrals over the film thickness are needed for both $Q(z,\Delta t)$ and $q(z)$ in order to make contact with experiment. We obtain

$$\frac{Q(\Delta t)}{2q}=1-\frac{\eta A\beta}{2q\gamma}\int_0^d \ln[1-H(z,\Delta t)]dz . \tag{8}$$

Since $q(z)$ is also proportional to η, the quantum efficiency for carrier generation cancels in Eq. (8). The dependence on the delay Δt is entirely given by $H(z,\Delta t)$. For weak pulses, with $B(z,0)\ll 1$, we need to retain only the $\exp(-\beta\Delta t)$ term in the Taylor expansion. For an optically thin film, $\alpha d \ll 1$, we have

$$\frac{Q(\Delta t)}{2q}=1+\frac{e^{-\beta\Delta t}}{[1+B]^2} , \tag{9}$$

where $B=\alpha I_0\tau\gamma/\beta$ is the constant exciton density. The double-pulse experiments at 355 nm correspond to an optically thick film with $\alpha=5.6\times10^4\ \mathrm{cm}^{-1}$, $d=3.4\times10^{-4}$ cm and exciton density B at the front face. The $d\to\infty$ limit is then appropriate and we find

$$\frac{Q(\Delta t)}{2q}=1+e^{-\beta\Delta t}\left[1-\frac{8B}{9}+\frac{103B^2}{108}+\frac{B^2e^{-\beta\Delta t}}{4}+\cdots\right] . \tag{10}$$

In either thin or thick films, the $\Delta t=0$ limit deviates from a simple quadratic dependence on the exciton concentration when B is finite.

Turning next to the dye laser experiments, we set $dn/dt=0$ in Eq. (1) since the 5-ns pulse width is long compared to the 600-ps exciton lifetime. The steady-state exciton density $n(z)$ at depth z is

$$n(r,z)=\frac{\frac{\beta}{2\gamma}Ce^{-\alpha z}}{[1+Ce^{-\alpha z}]^{1/2}+1} , \tag{11}$$

where $C=4\alpha\gamma I_0/\beta^2$ over the laser spot A. Since $n(z)$ is a function of αI_0, different combinations of α and I_0 are predicted to behave alike. The rate of carrier generation goes to the integral of $\gamma n(z)^2$ over the film thickness.

The (assumed) linear absorption leads to

$$N(\alpha d)=I_0(1-e^{-\alpha d}) \tag{12}$$

photons absorbed per second per unit area. The fraction of the excitons created that decays by exciton-exciton annihilation is

$$F(C,\alpha d)=\int_0^d \gamma n(z)^2 dz/N(\alpha d) . \tag{13}$$

The fraction corresponding to free carriers is $\eta F(C,\alpha d)$. The evaluation of F is straightforward for a laser pulse with uniform intensity and leads to

$$F(C,\alpha d)=\frac{\Gamma-4}{\Gamma}-\frac{4}{C(1-e^{-\alpha d})}\times\ln\left[1-\frac{(1-e^{-\alpha d})(\{C+1\}^{1/2}-1)}{\Gamma}\right] \tag{14}$$

with

$$\Gamma(C,d)=(C+1)^{1/2}+(Ce^{-\alpha d}+1)^{1/2} . \tag{15}$$

The dependence on the optical density αd is explicitly shown. In thin samples, Eq. (14) reduces to

$$F(C,\alpha d\ll 1)=\frac{(C+1)^{1/2}-1}{(C+1)^{1/2}+1} . \tag{16}$$

The lowest-order contribution is $C/4$ for $\alpha d\ll 1$, $C/8$ for $\alpha d\gg 1$, and all the expressions for $F(C,\alpha d)$ saturate at unity for large C.

IV. EXPERIMENTAL RESULTS

A. Steady-state experiments

The primary goal of the dye laser experiments originally was to determine the quantum efficiency for carrier generation as a function of photon energy and thus determine the free-carrier band gap as we had previously done in poly(methylpenylsilane).[8] When we found that the number of carriers generated was not a linear function of the incident light intensity, the number of measurements we had to make expanded greatly. We have measured the number of carriers generated as a function of the intensity of light by varying the light intensity by over an order of magnitude at more than 40 wavelengths between 392 and 210 nm. We also measured the amount of charge displaced at each wavelength and intensity with both polarities of the applied electric field, i.e., with the illuminated electrode both positive and negative.

The number of carriers generated per incident photon at a light intensity of 6×10^{11} photons/pulse as a function of photon energy is shown in Fig. 1. Also shown is the absorption spectrum of PDHS. The magnitude of the second peak in the absorption spectrum, at approximately 3.9 eV, is highly variable. It depends strongly on sample preparation and thermal history. Since our sample is too thick to measure the absorption spectrum we must remember that the absorption coefficient may be different from the value we use in this region. It should also be pointed out that the data plotted in Fig. 1 is more precisely the amount of charge displaced rather than the number of carriers created. The largest discrepancy will occur when the light is only weakly absorbed so that carriers are generated uniformly throughout the sample. In this situation the error would be a factor of 2 if the light is not reflected from the back electrode and any reflection will reduce the error. Since we know that a fairly large fraction is reflected but not how much, we decided to not try to correct any of the data.

The dashed line in Fig. 1 is the prediction of Eq. (14) using $\gamma=2\times10^{-7}$ cm^3 s^{-1}, $\beta=1.67\times10^{9}$ s^{-1}, a quantum efficiency for carrier generation by an exciton-exciton annihilation event $\eta=1.3\times10^{-3}$, a laser beam area of 0.4 cm^2 and a square laser pulse 5 ns long. The adjustable parameters are η and γ, whose magnitudes are discussed below.

We were also able to estimate the intensity dependence at a given wavelength and light intensity, approximating it as I^n. Least-square fits were made to log-log plots of the intensity dependence data and the exponent was evaluated as the slope at 6×10^{11} photons per pulse. The data obtained at 390.5 nm are shown in Fig. 2. The dashed line is the least-squares fit with a slope of 2.21 and the solid line was drawn with a slope of 2 for reference. The exponent n was also calculated using Eq. (14) and the above constants. The results are shown in Fig. 3. The errors are quite large, particularly at low photon energies, but the appropriate trends are clearly there. In retrospect it appears there may have been a small systematic error in our measurement of the light intensity at the lowest intensities but we have not tried to correct the data. Above 4.5 eV the data appear to depart from the theoretical predictions. We believe that band-to-band transitions are becoming important above 4.5 eV and will discuss those results in more detail below.

In order to use Eq. (14) we needed a measure of the absorption coefficient $\alpha(\omega)$ as a function of photon energy.

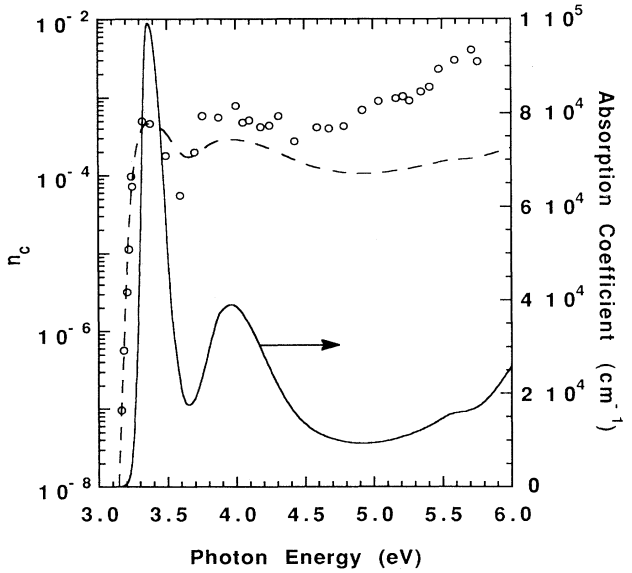

FIG. 1. The number of carriers generated per incident photon n_c versus photon energy. The dashed line is the prediction of Eq. (14) and the solid line is the absorption coefficient of PDHS which is provided for reference.

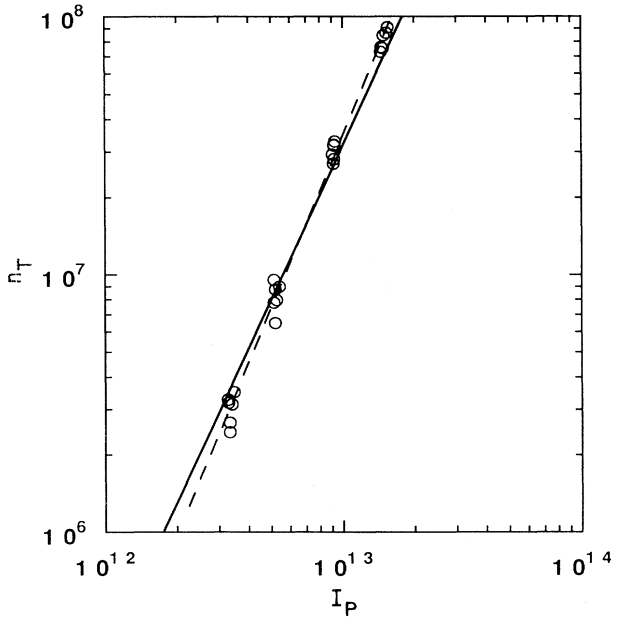

FIG. 2. The number of carriers generated per pulse n_T versus the light intensity I_p (units of photons per pulse) at 390.5 nm. The dashed line is a least-squares fit to the data with a slope of 2.21. The solid line is drawn with a slope of 2 for reference.

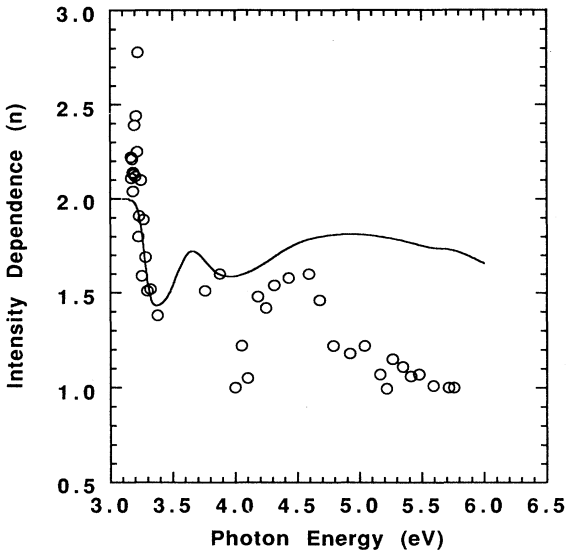

FIG. 3. Exponent n of the photocurrent intensity I^n, evaluated at 6×10^{11} photons per pulse. The open circles are the experimental results and the solid line is the prediction of Eq. (14).

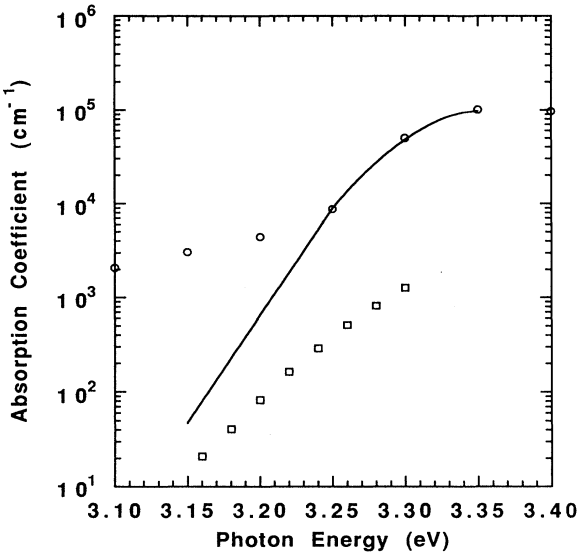

FIG. 4. The absorption coefficient of PDHS on the low-energy side of the exciton absorption band. The solid line is the curve we used. The open circles were obtained with a spectrophotometer and the open squares were obtained using photothermal deflection spectroscopy. See the text for an explanation of the discrepancies.

Above about 3.25 eV, the absorption coefficient is 10^4 cm^{-1} or greater, and it is relatively easy to simply measure the absorption spectrum of thin samples with a standard spectrophotometer and then measure the thickness of the film. Below 3.25 eV we have been unable to directly measure the absorption spectrum. Photothermal-deflection spectroscopy[24] was tried[23] but we concluded that the fluorescence quantum efficiency of PDHS is so high that most of the absorbed energy is radiated away rather than converted to heat, thus giving a too low $\alpha(\omega)$. We concluded that the best measure was our photoconductivity data. When the light is only weakly absorbed, the number of carriers generated should vary as $\alpha^2(\omega)$ if the carriers are generated by exciton-exciton annihilation and if the character of the excitons created does not change with photon energy. With these assumptions we obtained the absorption coefficient shown in Fig. 4. Also shown are some data from a standard spectrophotometer measurement and results from a photothermal-deflection spectroscopy experiment.

The agreement between experimental results at a light intensity of 4×10^{12} photons/pulse and theoretical predictions using the $\alpha(\omega)$ obtained this way is shown in Fig. 5. We show both the charge displaced when the illuminated electrode was positive (open circles) and that displaced when it was negative (open squares). In the experiments we were unable to see a significant difference between the two polarities below about 3.24 eV and the circles and squares are superimposed. The theoretical predictions of the rate equation, Eq. (1), are shown by the solid and dashed lines using the parameters quoted above. These results were obtained by numerical integration, keeping track of the charge displaced by each carrier generated. The fact that the squares are considerably above the dashed line indicates that more charge is displaced when

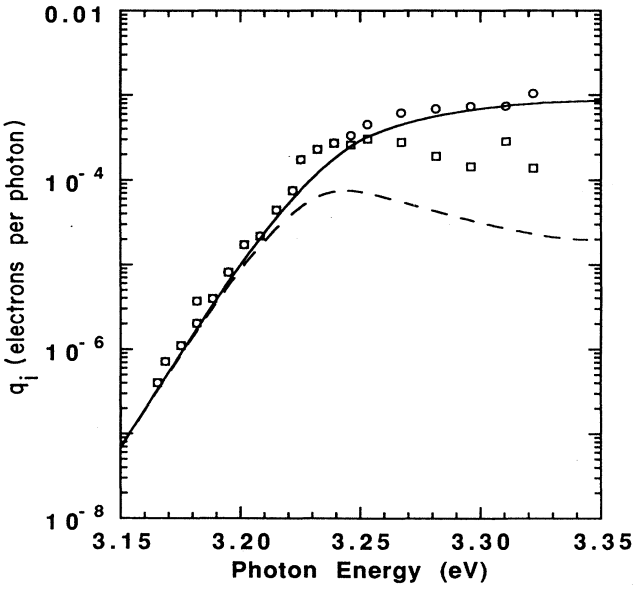

FIG. 5. The charge displaced per incident photon q_i at 4×10^{12} photons per pulse versus photon energy on the low-energy side of the exciton band. Data obtained when the positive electrode (circles) and the negative electrode (squares) were illuminated are shown. Below 3.24 eV the circles and squares are superimposed because the light passes through the sample with the little attenuation. The solid and dashed lines are numerical solutions of Eq. (1) for positive and negative electrode illumination, respectively.

the negative electrode is illuminated than the model predicts. The assumption is that only holes are mobile and the charge displaced when the negative electrode is illuminated results from holes created near the electrode moving to it. We have noted a similar discrepancy between the predictions of this hypothesis and experimental results in studies of photoconductivity in other polysilanes, but do not know its origin.

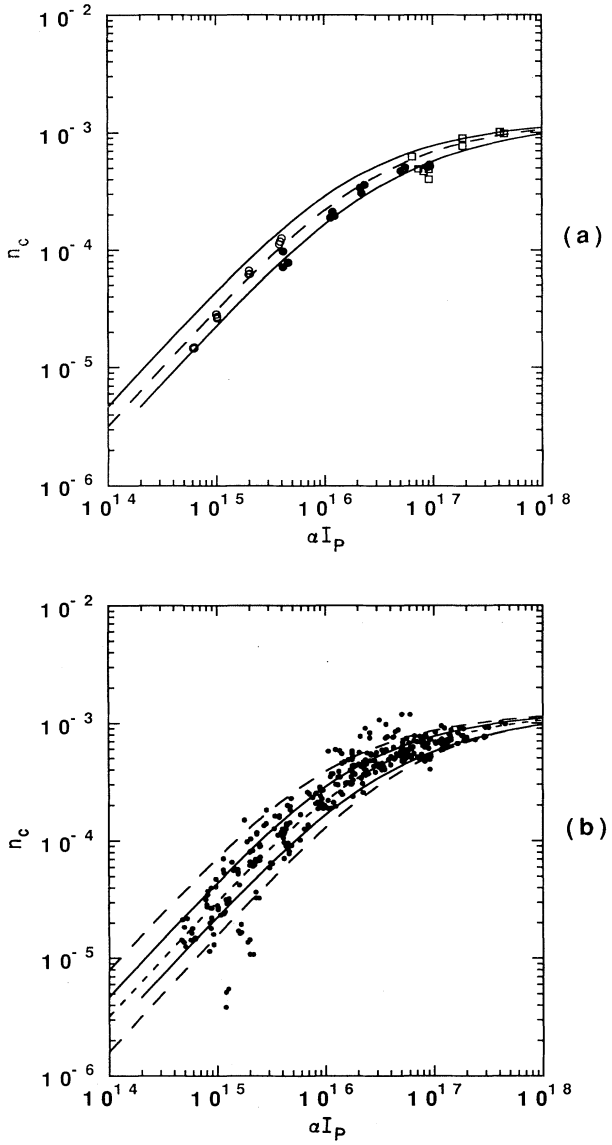

FIG. 6. The number of carriers generated per absorbed photon n_c versus the absorption coefficient times the light intensity (αI_p). (a) shows theoretical predictions and some representative data at 3.182 eV (open circles), 3.246 eV (solid circles), and 3.380 eV (open squares). The two solid lines and the dashed line between them were calculated using Eq. (14) with $\gamma=2\times10^{-7}$ $cm^3 s^{-1}$ and $\alpha d\rightarrow 0$ (upper solid line), $\alpha d=1$ (dashed line), and $\alpha d\rightarrow\infty$ (lower solid line). (b) shows all the data taken for photon energies less than 4.5 eV and the theoretical curves shown in (a). The added uppermost long-dashed line and the lowest long-dashed line were calculated using $\gamma=5\times10^{-7}$ $cm^{-3} s^{-1}$ and 1×10^{-7} $cm^3 s^{-1}$, respectively, with $\alpha d=1$.

Equation (14) shows that, except for a weak dependence on the optical density αd, *all* the steady-state results should simply be a function of αI_0. We have plotted in Fig. 6(a) representative results for $\alpha d<1$, ~ 1, and >1 for the number of carriers created at fixed wavelength and variable intensity. The asymptote fixes the quantum efficiency η for carrier generation at the applied field of 2×10^5 $V cm^{-1}$. The two solid lines in Fig. 6(a) are based on Eq. (14) for $\alpha d\gg 1$ and $\ll 1$, when it reduces to Eq. (15), with $\gamma=2\times10^{-7}$ $cm^3 s^{-1}$, $\eta=1.3\times10^{-3}$ and the independently known exciton lifetime $1/\beta=600$ ps. The dashed line corresponds to $\alpha d=1$. The dependence on αd is rather weak and beyond the present resolution.

We show in Fig. 6(b) a large fraction of our photoconductivity data at many wavelengths and intensities as a function of αI_0. The data at photon energies above 4.5 eV were omitted because band-to-band transitions then appear to be important. The full range of $\alpha(\omega)$ in Fig. 4 has been kept along with data at and above the exciton peak at 3.4 eV. The dashed and solid lines are again based on Eq. (14), with $\alpha d=1$, $\gg 1$, $\ll 1$, and the parameters used in Fig. 6(a). The fit over a broad range of wavelengths shows that $\gamma=2\times10^{-7}$ $cm^3 s^{-1}$ is independent of excitation energy, and this also appears to hold for $\eta=1.3\times10^{-3}$.

The exciton-exciton annihilation rate constant is in excellent agreement with the previous estimate of 1×10^{-7} $cm^3 s^{-1}$ based on fluorescence intensity measurements.[20] The dependence of Eq. (14) on γ is illustrated in Fig. 6(b) by taking the previous value of γ and $\alpha d=1$ for the lower long-dashed line. The upper long-dashed line corresponds to $\gamma=5\times10^{-7}$ $cm^3 s^{-1}$ and $\alpha d=1$. The fit is noticeably poorer in each case.

B. Double-pulse experiment

Perhaps the most convincing evidence that carriers are being generated by exciton-exciton annihilation is provided by our double-pulse experiments in which two, roughly equal intensity, 30-ps light pulses at 355 nm illuminate the sample and the number of carriers generated is measured as a function of the time delay Δt between the time of arrival of the two pulses. Figure 7 shows typical data from our earlier experiments in which we did not consciously control the polarization of the two light pulses. We plot against Δt the number of carriers generated by the two pulses divided by the sum of the number of carriers generated by the two pulses independently.

As discussed below, the exciton lifetime $1/\beta$ is not the only time dependence in Fig. 7 because PDHS is a crystalline polymer, while Eqs. (9) and (10) were derived for an isotropic medium with $\alpha d<1$ and >1, respectively, and $B(z,0)\ll 1$. For weak pulses, the predicted time dependence is $\exp(-\beta\Delta t)$ and the intercept in Fig. 7 depends on $B=\alpha I_0\tau\gamma/\beta$, which is γ/β times the exciton density at the front surface. We obtain $B=0.63$ in our experiments for $\gamma=2\times10^{-7}$ $cm^3 s^{-1}$ and 9.4×10^{10} photons cm^{-2} per 30-ps pulse. Thus even the weakest

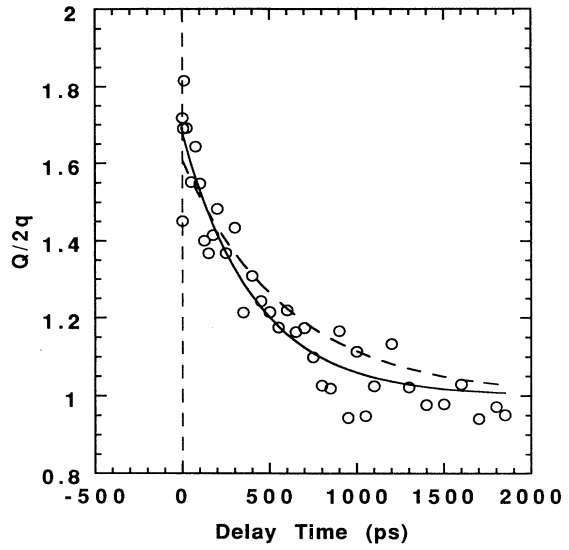

FIG. 7. The total charge generated by two 30-ps light pulses divided by the sum of the number of carriers generated by the two pulses independently versus the difference in the time of arrival of the two pulses. The solid line is a least-squares fit of Eq. (9) to the data, allowing both the lifetime and intercept to vary, and the dashed line is the least-squares fit obtained when the lifetime is constrained to be 600 ps.

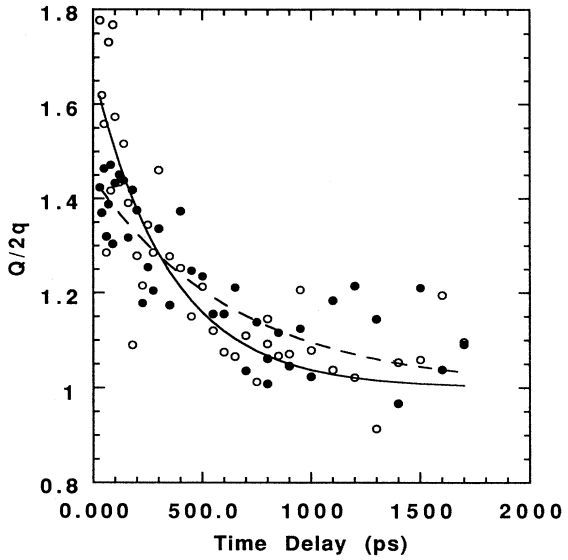

FIG. 8. The double-pulse experimental results with polarized light, open circles for parallel polarization of the two pulses and solid circles for perpendicular polarization. The solid and dashed lines are least-squares fits to the parallel and perpendicular polarization results, respectively.

pulses for measurable photocurrents lead to significant B and the estimated value of $Q/2q \sim 1.9$ from Eq. (10) at $\Delta t = 0$ is rather rough. Direct solution of Eq. (8) would be more accurate, but is not warranted at this stage.

The solid curve in Fig. 7 is a least-squares fit to an exponential with an adjustable intercept. The apparent exciton "lifetime" is 400 ps. The average lifetime obtained in five measurements is 380 ps, with a standard deviation of 65 ps. However, a 600-ps lifetime was found[22] from the fluorescence decay in thin PDHS films prepared from the same batch, independent of either the excitation or detection wavelength and consistent with previous PDHS lifetime results.[16] The dashed curve in Fig. 7 is the least-squares fit to a 600-ps decay.

We believe that we understand, at least qualitatively, the discrepancy between the apparent exciton lifetime determined in our double-pulse experiment and that determined from fluorescence time-dependence measurements. If we carefully control the polarization of the light in the two pulses and conduct experiments with the polarization of the two pulses parallel and with the polarizations perpendicular, we obtain different results. Some results are shown in Fig. 8. The solid line is a least-squares fit to the data obtained when the polarizations were parallel (open circles), and the dashed line is a least-squares fit to the data when the polarizations are perpendicular (solid circles). The parallel polarization lifetime obtained was 350 ps and that obtained with perpendicular polarization was 650 ps.

We believe the polarization dependence in Fig. 8 to be related to the crystallinity of PDHS. The transition dipoles for exciton generation are along segments to 10–30 Si atoms that form the polymer backbone. A pulse polarized along a hypothetical z axis consequently excites a $\cos^2\theta$ distribution of segments with azimuthal angle θ. The exciton distribution may nevertheless be taken to be isotropic, as assumed in Eq. (1), when the average separation between excitons is large compared to the segment length and the segments are randomly oriented. Crystalline domains of segments, on the contrary, require explicit consideration of the anisotropic distribution of excitons. The limit of large crystallites is again simple, since essentially all annihilation then occurs in a single crystallite and Eq. (1) can be used for each.

Crystallites of parallel segments have been shown to exist in PDHS.[25–27] We consider an x-polarized pulse on a PDHS film of thickness d. The exciton density $n(z,0)$ in Eq. (2) acquires a multiplicative factor of $\sin^2\theta\cos^2\varphi$ for a crystallite whose orientation is (θ,φ). The same multiplicative factor applies to $B(z,0)$ in Eq. (4). The charge carriers $q(z)$ at depth z for an isotropic distribution of large crystallites then require an additional angular average. The total number of carriers q generated by a single pulse is independent of the polarization.

For parallel or perpendicular polarization, respectively, the second pulse is x or y polarized. The previous development for the double-pulse experiment again leads to $Q(z,\Delta t)$ in Eq. (6). For crystallites with orientation (θ,φ), $H(z,\Delta t)$ is now given by

$$H(z,\Delta t)=\begin{cases}\dfrac{e^{-\beta\Delta t B'^2}}{(1+B')^2} & \text{(parallel)},\\[2ex] \dfrac{e^{-\beta\Delta t B'^2\tan^2\varphi}}{(1+B')(1+B'\tan^2\varphi)} & \text{(perpendicular)},\end{cases} \tag{17}$$

with $B'=B(z,0)\sin^2\theta\cos^2\varphi$. The integral over the film

thickness is carried out as before for weak pulses to obtain Eq. (10) for the crystallite. The angular average then leads, for $B' \ll 1$, to

$$\frac{Q(\Delta t)}{2q} = 1 + ae^{-\beta \Delta t} \tag{18}$$

with $a = 1$ and $\frac{1}{3}$, respectively, for parallel and perpendicular polarization. The lower intercept for perpendicular pulses reflects the more isotropic exciton distribution. The exciton lifetime nevertheless controls the decay when annihilation occurs within individual crystallites.

Differences between parallel and perpendicular pulses in Fig. 8 indicate that the segments in PDHS films form ordered domains or crystallites. The more rapid time dependence for parallel pulses indicates further that annihilation is not confined to individual crystallites. Physically, exciton diffusion out of crystallites excited by parallel pulses provides another mechanism besides unimolecular decay for decreasing the annihilation rate. The diffusion length $(zD/\beta)^{1/2}$ of the excitons on a lattice with coordination z seems to be comparable to the crystallite size in our films. We will return to this point in the Discussion, since γ provides an estimate of the diffusion constant and there are independent estimates for the PDHS crystallite sizes.

C. Free-carrier band-gap

As pointed out earlier, above about 4.5 eV it appears that one-photon processes begin to become important. Further evidence that this is the case is provided by comparing some measurements made at very low light intensity, where exciton-exciton annihilation can be excluded, with those made at high light intensity. In Fig. 9 we have plotted the number of carriers generated per incident photon as determined in an experiment using a xenon and a deuterium arc light source (open circles), as well as the data presented earlier in Fig. 1. The sample used for the low light intensity experiment was 19 μm thick, and it is likely that carrier trapping played a significant role in lowering the observed quantum efficiency. Nevertheless, the two data sets clearly approach one another near 4.5 eV and then the ratio between the two quantum efficiencies remains essentially constant, indicating that a linear process is dominant. However, there is no clear evidence of a distinct band gap. The quantum yield continues to rise strongly up to 6 eV as seen more clearly in the linear plot of Fig. 10. This graph suggests that the band gap might be best defined as about 5.2 eV based on a linear extrapolation of the high-energy data to the abscissa.

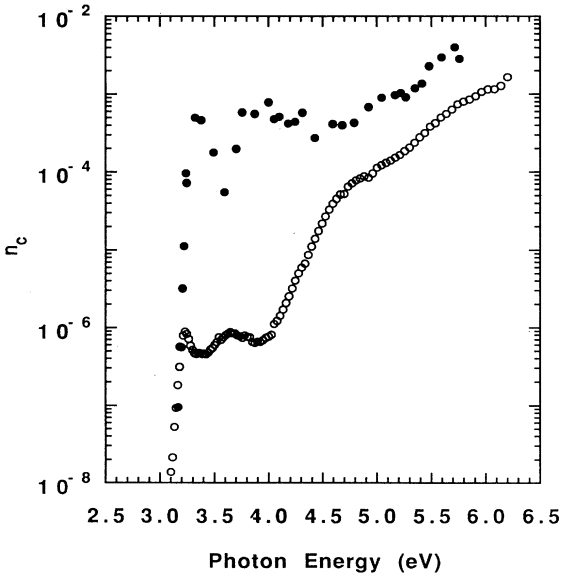

FIG. 9. Log-linear plot of the number of carriers generated per incident photon n_c versus photon energy at low (open circles) and high (solid circles) light intensity.

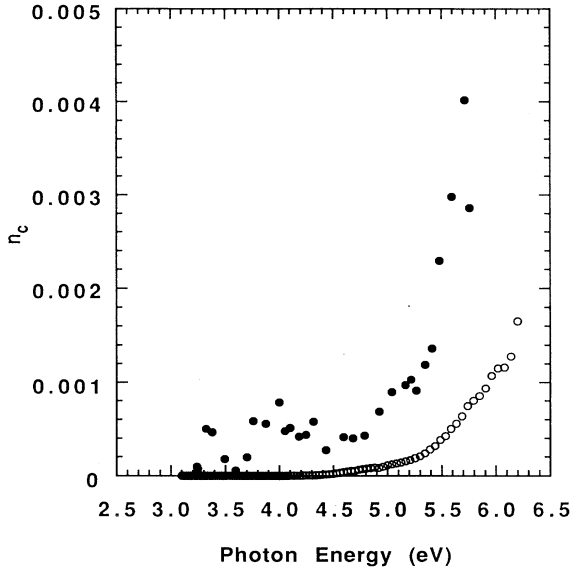

FIG. 10. Linear plot of the number of carriers generated per incident photon n_c versus photon energy at low (open circles) and high (solid circles) light intensity.

V. DISCUSSION

The photoconductivity data for PDHS films support and extend previous results for exciton-exciton annihilation. The annihilation rate constant is $\gamma = 2 \times 10^{-7}$ $cm^3 s^{-1}$ over a wide range of excitation energies, as shown in Fig. 6. As expected from Eq. (1), the annihilation rate depends on αI_0, which governs the exciton density created by the light, and on the optical density αd, which governs the exciton distribution in the film. The steady-state and double-pulse experiments are both consistent with Eq. (1). Moreover, the exciton lifetime $1/\beta$ is independently known. The quantum efficiency for carrier generation, 1.3×10^{-3} per exciton-exciton annihilation at a field of 2×10^5 V cm^{-1}, has been accurately determined and is typical for molecular systems in which geminate recombination dominates.[28] It is not clear, however, that geminate recombination alone accounts for the low quantum yield. Rapid decay of a highly excited state created

in the annihilation process, without creation of an electron-hole pair, could also be important.

The magnitude of γ is noteworthy for several reasons. First, it implies rapid exciton motion, even for excitons created in the red edge, and such excitons are clearly immobile in dilute solutions or glasses.[17] Second, γ in PDHS films is at least an order of magnitude larger than the annihilation constant in molecular crystals such as anthracene.[29] Third, the usual Förster mechanism for energy transfer must be reexamined to account for such large γ.

The relation $\gamma = 8\pi RD$ between exciton diffusion and annihilation is based on an isotropic random walk that terminates at the collision radius R.[30] We have $R \sim 0.5$ nm from the molecular size in anthracene. The corresponding dimension for an exciton in polymers is not obvious, but several experiments point to excitons associated with segments in PDHS. The narrow fluorescence is probably from the largest segments of 20–30 SI atoms in each strand of $\sim 10^4$ Si. Such "molecules" exceed 5 nm, along the chain, while the transverse dimension depends on the side groups. The conservative estimate of $R = 3$ nm still leads to $D = 0.05$ cm^2 s^{-1}. By comparison, the diffusion constant in crystalline anthracene[29] is $\sim 10^{-3}$ cm^2 s^{-1}.

Rapid exciton motion along the $(Si)_n$ backbone can be expected, since the all-*trans* segments are connected by, for example, gauche defects. Such intrachain motion is clearly implied by the fluorescence in dilute solution,[7] by fluorescence depolarization,[13–16] and by site-selective spectroscopy.[17] We believe such experiments probe excited-state relaxation on a chain isolated from others in a glass or solution rather than exciton motion that involves multiple chains as occurs in solid polymer films. Excitation at or above the exciton peak E_g, for example, migrates to the longest segments on a few ps. For isolated PDHS strands, intrachain transfers to longer and longer segments become progressively slower as the excitation energy is redshifted. The exciton becomes trapped when its 600-ps lifetime becomes less than the time between transfers.

Exciton motion leading to annihilation involves interstrand processes, as shown most simply by annihilation experiments on samples with shorter strands under conditions of fewer than one exciton generated per strand.[20] The energy independence of γ points to motion among long segments during the exciton's 600-ps lifetime, with negligible contributions in our experiments from the rapid initial excited-state relaxation. Photoconductivity has been observed down to 3.165 eV at 300 K, where α is estimated to be 100 cm^{-1}. Elschner *et al.*[17] have interpreted site-selective fluorescence in PDHS films at ~ 10 K to imply immobile excitons at 3.18 eV, where we estimate $\alpha \sim 225$ cm^{-1}. We believe their solution and glass data to be more compelling than the film results, but measurements under identical condition are needed. Previous fluorescence quenching studies showed no temperature dependence of γ down to 20 K in poly(*n*-propylmethylsilane).[19]

The photoconductivity of PDHS films thus points to interchain motion of excitons confined to long segments. The density of "long" segments is a matter of speculation, with 5%–10% an initial guess. The di-*n*-hexyl side groups effectively preclude overlap of the backbone wave functions. Dipole-dipole (Förster) transfer is a possibility. The usual formulation of point dipoles is inadequate, however, for segments of 20–30 Si atoms. As noted long ago by London[31] and illustrated by Knox for planar molecules,[32] major corrections to point dipoles occur when the molecular size exceeds the intermolecular separation. Long segments packed parallel to each other are expected to have the largest deviation, and dispersion forces[33] then go as r^{-3} rather than r^{-6} in the interstrand separation. One exciton on two parallel but nonoverlapping polyenes of 10 carbons at 0.4 nm leads to a transverse bandwidth[33] of ~ 0.5 eV. Since the bandwidth decreases with increasing length and is also sensitive to the relative orientation of the segments, we will not hazard an estimate for PDHS segments. But exciton motion between parallel segments is certainly faster than suggested by the point-dipole formula. Trommsdorf, Zeigler, and Hochstrasser[18] have estimated that excitation jump times should be less than 100 fs by apportioning the known transition dipole into N dipoles of magnitude $\mu/N^{1/2}$, one at each Si site and calculating the dipole-dipole interaction between these minidipoles on adjacent segments.

Interstrand exciton motion brings us to consider polymer morphology, which has already been alluded to in the analysis of the polarization dependence of the double-pulse experiment in Fig. 8. Polymer morphology is an active current area of research. Carefully prepared PDHS films have a ribbonlike morphology, containing crystallites with widths of ~ 100 nm and lengths in the micrometer range.[27] They are unusually large for polymers. Since the polymer strands were found to be parallel to the width and perpendicular to the length, it was concluded that the 100-nm width corresponds to the lamella thickness. We obtain a diffusion length $(zD/\beta)^{1/2}$ of 100 nm for $z = 4$ and two-dimensional motion in films whose morphology has not been characterized, but whose lamella are probably several tens of nm thick. The faster decay for parallel pulses is quite consistent with $D \sim 0.05$ cm^2 s^{-1} found from $\gamma = 2 \times 10^{-7}$ cm^3 s^{-1}.

As was pointed out at the end of the Experimental Results section, a large increase in the quantum efficiency for carrier generation begins at about 5.2 eV, suggesting that there is a free-carrier band gap. Further evidence for this interpretation may be provided by the observation of Tachibana *et al.*[34] of a very large electroabsorption signal beginning at about 5.2 eV. Tachibana *et al.* assigned the signal to a highly delocalized exciton, and argued against an assignment to an interband transition on the basis that they did not observe an expected electric field dependence of the line shape.

VI. SUMMARY

We have shown that charge carriers are generated in solid films of PDHS by exciton-exciton annihilation and that the quantum efficiency is about 1.3×10^{-3} per an-

nihilation. Using this phenomenon, we have shown that the exciton-exciton annihilation rate constant γ is 2×10^{-7} cm^3 s^{-1}, in excellent agreement with the results we obtained previously by studying the fluorescence intensity versus exciting light intensity. We also showed that at ambient temperature γ is independent of the energy of the exciting photons, even at energies far out on the low-energy side of the exciton absorption band. Using two 30-ps pulses we showed that the excitons remain mobile throughout their 600-ps lifetime and that they diffuse distances comparable to crystallite sizes in the polycrystalline polymer films, probably on the order of tens of nanometers. The magnitude of γ suggests that the exciton diffusion coefficient D is about 0.05 cm^2 s^{-1}, and that thus $(zD/\beta)^{1/2}\sim100$ nm, consistent with the above observation. We also reported that measurements of the photon energy dependence of the quantum efficiency for carrier generation suggests that the band gap for carrier generation is 5.2 eV.

ACKNOWLEDGMENTS

The technical assistance of Paul Beeson is gratefully acknowledged. The photothermal deflection spectroscopy measurements were provided by C. H. Seager, and J. R. G. Thorne made the fluorescence lifetime measurements. Polymer samples were provided by J. M. Zeigler. The work at Sandia National Laboratories was supported by the U.S. Department of Energy under Contract No. DE-AC04-76DP00789 and the work of Princeton University was partially supported by NSF Grant No. NSF-DMR-8921072.

[1]J. H. Burroughes, D. D. C. Bradley, A. R. Brown, R. N. Marks, K. Mackay, R. H. Friend, P. L. Burns, and A. B. Holmes, Nature (London) **347**, 539 (1990).
[2]D. Braun and A. J. Heeger, Appl. Phys. Lett. **58**, 1982 (1991).
[3]Z. G. Soos and R. G. Kepler, Phys. Rev. B **43**, 11 908 (1991).
[4]R. G. Kepler and Z. G. Soos, Phys. Rev. B **43**, 12 530 (1991).
[5]R. G. Kepler and Z. G. Soos, in *Electrical, Optical and Magnetic Properties of Organic Solid State Materials,* edited by L. Y. Chiang, A. F. Garito, and D. J. Sandman, Symposium Proceedings Series, Vol. 247 (Materials Research Society, Pittsburgh, PA, 1992), p. 655.
[6]R. D. Miller and J. Michl, Chem. Rev. **89**, 1359 (1989)
[7]L. A. Harrah and J. M. Ziegler, in *Photophysics of Polymers,* edited by C. E. Hoyle and J. M. Torkelson, ACS Symposium Series Vol. 358 (American Chemical Society, Washington, DC, 1987), p. 482.
[8]R. G. Kepler, J. M. Zeigler, L. A. Harrah, and S. R. Kurtz, Phys. Rev. B **35**, 2818 (1987).
[9]M. A. Abkowitz, M. J. Rice, and M. Stolka, Philos. Mag. B **61**, 25 (1990).
[10]C. Sandorfy, Can. J. Chem. **33**, 1337 (1955).
[11]Z. G. Soos and G. W. Hayden, Chem. Phys. **143**, 199 (1990).
[12]K. S. Schweizer, in *Silicon-Based Polymer Science: A Comprehensive Resource,* edited by J. M. Zeigler and F. W. G. Fearon, Advances in Chemistry Series Vol. 224 (American Chemical Society, Washington, DC, 1990), p. 379.
[13]K. A. Klingensmith, J. W. Downing, R. D. Miller, and J. Michl, J. Am. Chem. Soc. **108**, 7438 (1986).
[14]J. Michl, J. W. Downing, T. Karatsu, K. A. Klingensmith, G. M. Wallraff, and R. D. Miller, in *Inorganic and Organometallic Polymers: Macromolecules Containing Silicon, Phosphorus, and Other Inorganic Elements,* edited by M. Zeldman, K. J. Wynne, and H. R. Allcock, ACS Symposium Series Vol. 360 (American Chemical Society, Washington, DC, 1988), p. 61.
[15]Y. R. Kim, M. Lee, J. R. G. Thorne, R. M. Hochstrasser, and J. M. Zeigler, Chem. Phys. Lett. **145**, 75 (1988).
[16]J. R. G. Thorne, R. M. Hochstrasser, and J. M. Zeigler, J. Phys. Chem. **92**, 4275 (1988).
[17]A. Elschner, R. F. Mahrt, L. Pautmeier, H. Bassler, and M. Stolka, Chem. Phys. **150**, 81 (1991).
[18]H. P. Trommsdorff, J. M. Zeigler, and R. M. Hochstrasser, Chem. Phys. Lett. **154**, 463 (1989).
[19]R. G. Kepler, Synth. Met. **28**, C573 (1989).
[20]R. G. Kepler and J. M. Zeigler, Mol. Cryst. Liq. Cryst. **175**, 85 (1989).
[21]R. G. Kepler and J. M. Zeigler, in *Silicon-Based Polymer Science: A Comprehensive Resource,* edited by J. M. Zeigler and F. W. G. Fearon, Advances in Chemistry Series Vol. 224 (American Chemical Society, Washington, DC, 1990), p. 459.
[22]R. G. Kepler, Z. G. Soos, and J. R. G. Thorne, Synth. Met. **54**, 391 (1992).
[23]R. G. Kepler, C. H. Seager, Z. G. Soos, and P. C. M. McWilliams, Synth. Met. **50**, 387 (1992).
[24]C. H. Seager and C. E. Land, Appl. Phys. Lett. **45**, 395 (1984).
[25]A. J. Lovinger, F. C. Schilling, F. A. Bovey, and J. M. Zeigler, Macromolecules **19**, 2657 (1986).
[26]F. C. Schilling, F. A. Bovey, A. J. Lovinger, and J. M. Zeigler, Macromolecules **19**, 2660 (1986).
[27]F. C. Schilling, F. A. Bovey, A. J. Lovinger, and J. M. Zeigler, in *Silicon Based Polymer Science,* edited by J. M. Zeigler and F. W. G. Fearon, Advances in Chemistry Series Vol. 224 (American Chemical Society, Washington, DC, 1990), p. 341.
[28]M. Pope and C. E. Swenberg, *Electronic Processes in Organic Crystals* (Clarendon, Oxford, 1982), p. 484.
[29]R. G. Kepler, in *Treatise on Solid State Chemistry,* edited by N. B. Hannay (Plenum, New York, 1976), Vol. 3, p. 636.
[30]S. Chandrasekhar, Rev. Mod. Phys. **15**, 1 (1943).
[31]F. London, J. Chem. Phys. **46**, 305 (1942).
[32]R. S. Knox, in *Bioenergetics of Photosynthesis,* edited by Govindjee (Academic, New York, 1975), p. 202.
[33]Z. G. Soos, G. W. Hayden, P. C. M. McWilliams, and S. Etemad, J. Chem. Phys. **93**, 7439 (1990).
[34]H. Tachibana, Y. Kawabata, S.-Y. Koshihara, and Y. Tokura, Solid State Commun. **75**, 5 (1990).